device (e.g.: maximum enhancement is achieved at zero extinction or critical coupling condition).

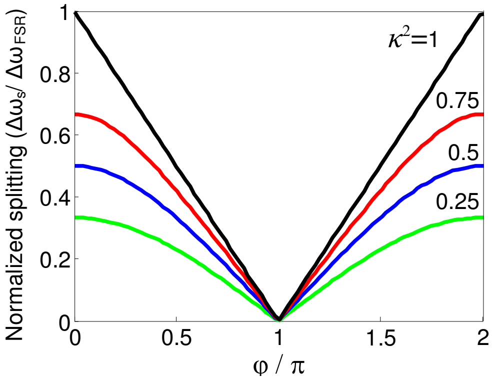

Fig. 3. Normalized frequency splitting versus the phase difference between the two arms of the interferometer coupling the two resonators in the two-point-coupled structure shown in Fig. 1(c). Numbers over the curves indicate the value of κ^2. In these simulations we change the phase difference between the two arms of the Mach-Zehnder resonator (Arm1 and Arm2 in Fig. 1(c)). All other parameters in these simulations are the same as those in the caption of Fig. 2.

As field enhancement is one of the more important measures in many sensing and nonlinear optics applications, the effect of resonator mutual coupling on field enhancement is studied in section 4 in detail.

3. Fabrication and experimental results

To experimentally demonstrate the proposed idea, the coupled-resonator device with two-point-coupling is fabricated on an SOI wafer with silicon slab thickness of 230 nm, and a 1µm thick buried oxide (BOX) layer (Fig. 4). Microheaters are integrated on the MZI to tune the coupling between the resonators. The width of the waveguides throughout the device is 480 nm to assure single-mode operation. The length of each resonator is 245 µm (including MZI length) and each arm of the Mach-Zehnder interferometer is 60 µm long. The DCs are identical and the gap and length of the parallel coupling region is 150 nm and 7.5 µm, respectively. The pattern of the device is written on ZEP electron-beam resist using electron-beam lithography (JEOL 9300) and etched in silicon by inductively-coupled-plasma (STS ICP) using a Cl_2-based chemistry. After this step, 1 µm SiO2 is deposited using plasma-enhanced chemical-vapor-deposition (PECVD) and microheater patterns are defined by a lift-off process using ZEP and electron-beam evaporation. Optimized microheaters with rapid reconfiguration have been developed to achieve sub-microsecond reconfiguration [5]. Microheaters are composed of 75 nm thick nickel and contact pads are covered with 150 nm gold for better electrical contact. Single-step lift-off of both nickel and gold is performed at the locations of the heaters and contact pads. In another lithography step, areas over microheaters are opened using ZEP resist, and gold is removed using nickel-safe GE-8148 gold etchant (Transene Inc.).

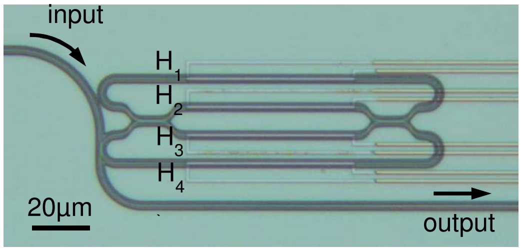

Fig. 4. Optical micrograph of the two-point-coupled resonator structure fabricated on SOI with integrated microheaters. H_1, H_2, H_3, and H_4 show the microheaters fabricated on top of the structure for thermal tuning.

Figure 4 shows the optical micrograph of the photonic device with integrated microheaters. Separate heaters are allocated to different parts of the device for independent control over coupling and resonance wavelength.

The transmission is measured by coupling light into and out of the device using tapered fibers in a standard optical characterization test setup. The TE-polarized light is incident on the device from a swept-wavelength tunable laser and the output of the device is coupled into a photodetector and the data is transferred to the PC using a data-acquisition (DAQ) card. Figure 5(a) shows the transmission spectrum of the device shown in Fig. 4. It is observed that two sets of modes with similar FSR of about 2.3 nm are present in the spectrum. This FSR corresponds to the FSR of each single resonator (which is 2.3 nm). Also, the spacing between two adjacent modes from different sets corresponds to the mode splitting of the otherwise degenerate modes of the resonators. Because of the high level of coupling, modes of the two resonators are strongly split by approximately 0.86 nm. From this amount of splitting, power coupling coefficient of each DC between the two resonators is calculated to be $\kappa^2 = 0.42$, assuming the two couplers are identical. Intrinsic Q of the modes of the coupled-resonator structure is also measured to be 70,000.

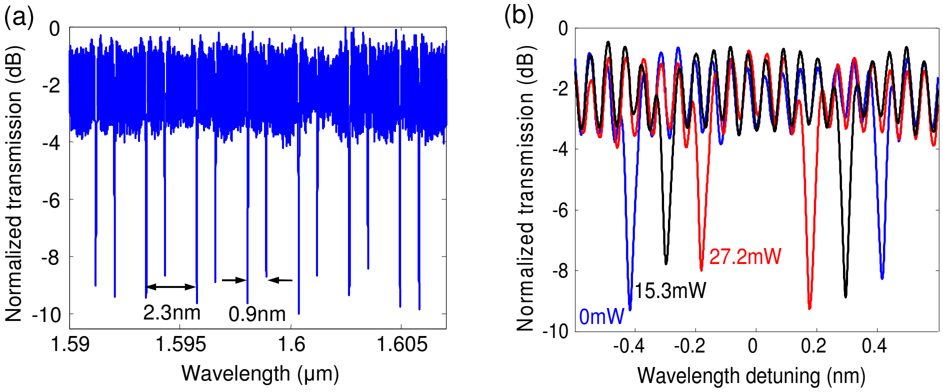

Fig. 5. (a) Normalized transmission spectrum of the coupled resonator structure shown in Fig. 4. (b) Normalized transmission spectra of the two coupled modes near $\lambda = 1.601$ μm for different power dissipations in heater H_2 (Fig. 4). Horizontal axis is wavelength detuning with respect to the center of the two coupled modes. A wavelength offset is added to the data to compensate for the red-shift in the resonance wavelengths of the modes in the coupled-resonator structure.

By heating the upper interferometer arm through heater H_2 (Fig. 4), coupling between the two resonators can be tuned. Figure 5(b) depicts the normalized transmission spectra of the two coupled resonance modes in the vicinity of $\lambda = 1.601$ μm for three different levels of power dissipation in heater H_2. The number next to each spectrum is the power dissipation in the microheater. Similar tuning results are obtained for other FSRs in Fig. 5(a). Horizontal

#124039 - $15.00 USD Received 17 Feb 2010; revised 11 Apr 2010; accepted 16 Apr 2010; published 21 Apr 2010
(C) 2010 OSA

axis in Fig. 5(b) shows the wavelength detuning from the center of the coupled modes (or supermodes). It is observed that as the phase mismatch between the arms of the interferometer is increased (through applying heat), coupling between the resonators and consequently the mode spacing between the coupled modes is decreased. In addition to the change in the resonator coupling strengths, resonance wavelength of the upper resonator is red-shifted while heating the upper interferometer arm. This causes the center of the two coupled resonant modes (even and odd supermodes) to be red-shifted as their spacing is reduced. Here, this red-shift is compensated by introducing an appropriate wavelength offset to the experimental data, so that the centers of coupled-modes in each transmission spectrum match. In practice, by simultaneous tuning of all fabricated heaters, center wavelength of two resonators can remain unchanged while their mutual coupling is tuned. Figure 6 shows the change in resonance wavelength spacing of the even and odd coupled-modes for the structure in Fig. 4 for different power dissipations in heater H_2. It is observed that 0.4 nm change in wavelength spacing between coupled modes is achieved by dissipating 27 mW in H_2. This amount of change is equivalent to 20% of the FSR of the uncoupled resonators.

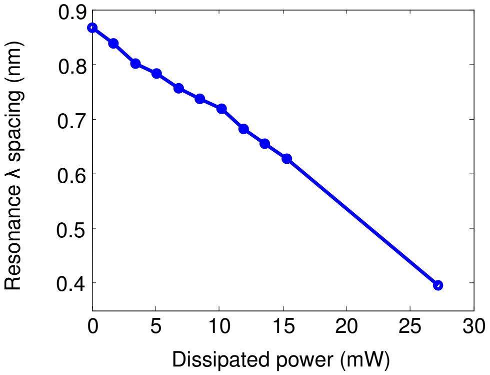

Fig. 6. Resonance wavelength spacing versus power dissipation in heater H_2 for the structure shown in Fig. 4.

4. Discussion

The results shown in Section 3 clearly show that the spacing of the adjacent modes of the resonator-based device can be tuned by a relatively large amount by using a single heater. The fact that the splitting between adjacent modes in Fig. 4 can change from 0.86 nm (zero power dissipation) to 0.4 nm (equal to 20% of an FSR) with only 27 mW heating power dissipation in H_2, proves that the resonator-based device in Fig. 4 can be used for a large set of signal conditions in applications like nonlinear optics in which signals with different wavelengths interact. By tuning the mode spacing, we can achieve resonance condition and simultaneous field enhancement for the involved signals. The amount of field-enhancement is an important characteristic which determines the device performance and needs to be addressed for any proposed device. As our proposed resonator structure is composed of an interferometer in addition to resonators, its field-enhancement characteristic is expected to be different compared to a simple resonator. Using a similar transfer-matrix approach as in Ref [13], field-enhancement of the even and odd supermodes in the two resonators of the two-point-coupled structure (Fig. 1(c)) are calculated as a function of phase difference between the two arms of the interferometer, and the results are shown in Fig. 7. In these simulations, the total lengths of both resonators are 245 μm; the lengths of the interferometer arms are 60 μm; the power coupling coefficients of DCs between the two resonators are $\kappa^2 = 0.7$; and the power coupling coefficient for the coupling of the bus waveguide to the lower resonator is $\kappa_{ex}^2 = 0.09$ (close to the critical coupling condition for an intrinsic Q of 10^5). The intensity enhancements shown in Fig. 7 are denoted by a and defined by the ratio of the intensity of the field of each resonant mode inside the resonator to the intensity of the field at the input waveguide. Subscripts 1 and

#124039 - $15.00 USD   Received 17 Feb 2010; revised 11 Apr 2010; accepted 16 Apr 2010; published 21 Apr 2010
(C) 2010 OSA

2 determine the fields in the bottom resonator (R_1) and the top resonator (R_2), respectively. Also, the modes with lower and higher frequency are called even and odd mode, respectively. Figure 7 shows that as the MZI phase difference increases, the amount of enhancement of the even (odd) mode in R_1 increases (decreases) until $\varphi = 0.8\pi$. As φ further increases, R_2 becomes decoupled from R_1; the field in R_2 drops to zero; and the enhancement of both even and odd modes increases in R_1. The reason for this high increase in the field-enhancement is because of the decrease in the effective length of the coupled-resonator system as the resonators are decoupled. This decrease in the effective length results in the decrease of the mode-volume of the structure, which directly translates into a higher field enhancement. In simulations, as φ approaches π, even and odd modes gradually overlap and become numerically indistinguishable. In Fig. 7, the dashed lines connect the last simulation point for which even and odd modes were distinguishable (i.e., $\varphi = 0.95\pi$) to the limiting case of zero coupling (i.e., $\varphi = \pi$), where the two modes completely overlap. It is observed that in each resonator (R_1 and R_2) both even and odd modes exhibit field enhancement simultaneously. This confirms that waves in resonance with these modes exhibit enhanced nonlinear interaction. However, this enhancement varies as the resonance frequency spacing is tuned and this has to be taken into account for any application.

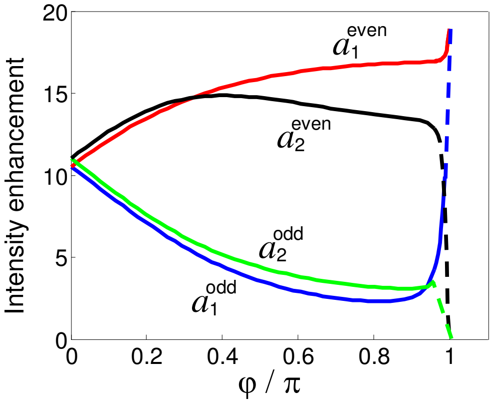

Fig. 7. Intensity enhancement of even and odd supermodes in R_1 (bottom resonator) and R_2 (top resonator) as a function of the phase difference between the interferometer arms in Fig. 1(c). Dashed parts of each curve connects the last simulation data-point for which the odd and even modes could be resolved, to the final value at π phase-shift (uncoupled case).

5. Conclusion

In conclusion, we have theoretically and experimentally demonstrated a coupled-resonator device in which the spacing between its adjacent modes can be tuned through tuning of their mutual coupling. The device was fabricated on an SOI platform with integrated microheaters for the purpose of tuning. By over-coupling the two resonators, a mode splitting as high as 0.86 nm (0.374xFSR) is achieved and this splitting was tuned down to 0.4 nm by heating one arm of the interferometer coupling the two resonators. To the best of our knowledge this is the first demonstration of a resonator-based device in an integrated platform in which the spacing between the adjacent resonance modes is tuned by 20% of its FSR. Through numerical simulations we have also shown that both of the split supermodes exhibit high field enhancements, which is the requirement for nonlinear optics and sensing applications.

Appendix A. Resonance condition of the coupled-resonator device

Here, we derive the resonance condition of the device shown in Fig. 1(a) using the transfer-matrix method [13]. If we assume that the vectors $\overline{a} = [a_2\ a_1]^T$ and $\overline{b} = [b_2\ b_1]^T$ in Fig. 1(a) represent the wave amplitudes entering and exiting the DC, respectively; we have [12]

$$\overline{b} = \mathbf{T}\overline{a} = e^{-j\theta_c}\begin{bmatrix} t_c & j\kappa_c \\ j\kappa_c^* & t_c^* \end{bmatrix}\overline{a} \quad , \tag{1}$$

where **T** is the transfer matrix of a general DC coupling the two resonators in which θ_c is the propagation phase, and t_c and κ_c are the amplitude through and cross-coupling coefficients, respectively. Also, through the feedback path from $\overline{b}$ to $\overline{a}$ we have

$$\overline{a} = e^{-j\beta L}\overline{b} \quad , \tag{2}$$

where L is the length of each resonator and β is propagation constant of resonators. By combining Eqs. (1) and (2) we have

$$\left|\mathbf{T} - e^{j\beta L}\mathbf{I}\right| = 0 \quad , \tag{3}$$

and by substituting for **T** from Eq. (1) in Eq. (3), the following eigenvalue equation for the resonance frequency of the coupled-resonator device is derived:

$$e^{j2\phi} + 2\,\mathrm{Re}\{t_c\}e^{j\phi} + 1 = 0 \quad . \tag{4}$$

Here, $\varphi = \theta_c + \beta L$ and Re{.} represents the real part of the argument in the parentheses. It should be noted that since very strong coupling between resonators is considered, first-order coupled-mode-theory could not be used here [2].

Figures 1(b) and 1(c) show the two coupled-resonator structures of our interest in which coupling is achieved using one and two symmetric DCs, respectively. The power through and coupling coefficients of all DCs in both structures are denoted by t^2 and κ^2, respectively. For the coupler in the single-point-coupled resonator (Fig. 1(b)), we have

$$t_c = t, \quad \kappa_c = k, \quad \theta_c = 0, \tag{5}$$

and for the MZI coupler in the two-point-coupled resonator (Fig. 1(c)), we have,

$$t_c = t^2 e^{-j\Delta\phi_{MZ}/2} - k^2 e^{j\Delta\phi_{MZ}/2}, \quad \kappa_c = 2kt\cos\left(\Delta\phi_{MZ}/2\right), \quad \theta_c = \phi_{MZ}^{ave}, \tag{6}$$

where, $\Delta\phi^{MZ} = \phi_1^{MZ} - \phi_2^{MZ}$ and $\phi_{ave}^{MZ} = \left(\phi_1^{MZ} + \phi_2^{MZ}\right)/2$; where, ϕ_1^{MZ} and ϕ_2^{MZ} are the propagation phase terms in Arm1 and Arm2 of the Mach-Zehnder, respectively. By substituting Eqs. (5) and (6) into Eq. (3) and by solving the eigenvalue equation, resonance frequencies of the coupled-resonator structures and consequently, their resonance splitting are calculated and shown in Fig. 1(d).

Acknowledgments

This work was supported by Air Force Office of Scientific Research under Contract No. FA9550-07-1-0201 (G. Pomrenke).